Linearized General Relativity in hyperboloidal slices (Extended Abstract)

Inês Rainho
CENTRA, Departamento de Física, Instituto Superior Técnico – IST, Universidade de Lisboa – UL, Avenida Rovisco Pais 1, 1049 Lisboa, Portugal

Future null infinity is the only location in spacetime where gravitational radiation can be unambiguously measured, and is also the appropriate idealization of observers of astrophysical events. The accuracy of the waveforms extracted from numerical simulations is crucial to estimate the correct properties of the sources of gravitational radiation detected by the interferometers. Currently, these waveforms are computed by either extrapolation or Cauchy-characteristic extraction/evolution. However, these methods are unsatisfactory from a first principles perspective. We take an alternative approach – the hyperboloidal method – in which spacetime is foliated into spacelike hypersurfaces that reach future null infinity. We introduce new coordinates that compactify spacetime, and in which the wave equations have formally singular terms. We can be overcome these singularities by considering the rate of decay of the fields and rescaling them properly. To better understand the decay of the fields, we introduce the good-ugly model and show that it reproduces the behavior of the linearized Einstein equations. We implement the hyperboloidal approach for the model equations and show that they are regular at future null infinity. For the numerical implementation, we use the NRPy+ code, and solve the equations in first-order in time and space with axially symmetric initial data on a staggered grid. Clean convergence is found, indicating a successful result. A similar approach can be done for full General Relativity, albeit with additional complications.

1. INTRODUCTION

General Relativity (GR) is the most successful theory of gravity. It predicts the existence of gravitational waves (GWs), which were directly detected for the first time in 2015 by the Laser Interferometer Gravitational-Wave Observatory (LIGO) [1, 2]. Since then, GWs have been detected frequently, and have brought with them information about the universe. These detections gave very strong evidence for the existence of black holes (BHs), and, along with their electromagnetic counterpart, imposed constraints on modified theories of gravity [3].

The data gathered by GW detectors is compared with waveforms obtained from numerical simulations to recover the properties of the systems that emitted the signal. The waveforms are obtained by evolving the system using the Einstein field equations (EFE), and extracting the emitted signals. Gravitational radiation is only unambiguously defined at future null infinity ($\mathscr{I}^+$), the "location" in spacetime where light rays arrive, and which also corresponds to the correct idealization of astrophysical observers. The most common way to obtain the waveforms is to compute the relevant quantities at several radii and perform an extrapolation to future null infinity, which is not optimal, since it does not allow for the extraction of signals directly at $\mathscr{I}^+$. Another common approach is called Cauchy-characteristic extraction/evolution (CCE), in which spacetime is divided into a Cauchy and a characteristic domain reaching null infinity, separated by an unphysical boundary. If we evolve for a long enough period of time, the waveform gets affected by the reflections at the unphysical boundary, which is not satisfactory from a first principles viewpoint.

A possible solution to this problem is the use of hyperboloidal slices, which are spacelike and smooth everywhere, and, by definition, reach future null infinity, allowing us to unambiguously extract gravitational waves. In practice, evolving on hyperboloidal slices requires writing the EFE in a new set of coordinates adapted to outgoing waves. By performing this coordinate transformation, infinity is brought to a finite coordinate distance. This introduces infinities in the equations themselves, but they can be overcome by considering the rate of decay of the fields as we approach future null infinity.

2. HYPERBOLOIDAL COMPACTIFICATION

In order to foliate spacetime into hyperboloidal slices, we need to perform a hyperboloidal compactification, i.e. introduce hyperboloidal coordinates that bring $\mathscr{I}^+$ to a finite coordinate distance. This is done in two steps: selecting a time parameter whose level sets are hyperboloidal slices (hyperboloidal time), and bringing in the compactification of the radial coordinate on those slices. A detailed discussion of this process can be found in [4].

Let us consider the example of the hyperboloidal compactification of Minkowski spacetime and its use with the wave equation. We can bring spatial infinity to a finite coordinate distance by performing a compactification in the outgoing direction, R. We introduce a compactifying coordinate r such that $R = \frac{r}{\Omega(r)}$, and require that the gradient of $\Omega(r)$ does not vanish when $\Omega(r) = 0$, which corresponds to infinity in R. We could also do this for a Cauchy slice, but the loss of resolution of signals propagating near spatial infinity creates numerical problems and, besides, we are not reaching $\mathscr{I}^+$. With that in mind, we also need to introduce a new time coordinate, t, to ensure that the slices reach $\mathscr{I}^+$ – not just spatial infinity (i_0) –, and to avoid loss of resolution. We, therefore, define t as

$$t = T - H(r)\,, \tag{1}$$

where T is the usual time, and $H(r)$, known as the

height function, must satisfy $|dH/dR| < 1$ so that t is a time function.

Consider the case of 1+1 dimensions. The wave equation reads

$$(-\partial_T^2 + \partial_R^2)\psi = 0\,. \tag{2}$$

In compactified hyperboloidal coordinates, this turns into

$$\left[\partial_t^2 + \frac{\Omega^2}{(1-h^2)L}\left(2h\partial_t\partial_r - \frac{\Omega^2}{L}\partial_r^2 + \partial_r h\partial_t - \partial_r\frac{\Omega^2}{L}\partial_r\right)\right]\psi = 0\,, \tag{3}$$

where $h \equiv \frac{dH}{dR}(r)$ and $L \equiv \Omega - r\frac{d\Omega}{dr}$. We choose $H(R) = \sqrt{S^2 + R^2}$ and set the compress function to

$$\Omega = \frac{1}{2}\left(1 - \frac{r^2}{S^2}\right)\,. \tag{4}$$

Thus, $S = \pm r$ is the coordinate location of null infinity, where the wave equations become

$$\partial_t(\partial_t \pm 2\partial_r)\psi = 0\,, \tag{5}$$

which indicates that both boundaries are outflow, and boundary conditions are not needed to solve the partial differential equation problem.

In multiple spatial dimensions, the regularization of the equations at future null infinity is not as straightforward. In 3+1 dimensions, the scalar wave equation in spherical coordinates (T, R, θ, ϕ) is

$$\left(-\partial_T^2 + \partial_R^2 + \frac{2}{R}\partial_R + \frac{1}{R^2}\Delta_{\mathbb{S}^2}\right)\psi = 0\,, \tag{6}$$

where $\Delta_{\mathbb{S}^2}$ is the Laplace operator on the 2-sphere. The angular term admits a regular compactification since, under compactification, it is multiplied by Ω^2, whereas the first radial derivative term leads to a singular operator at infinity. This problem can be solved by rescaling the field such that it attains a non-vanishing finite limit at future null infinity. In three spatial dimensions, fields that satisfy the wave equation decay as R^{-2}. We define the rescaled field $\Psi = R\psi$. The wave equation for this new variable is

$$\left(-\partial_T^2 + \partial_R^2 + \frac{1}{R^2}\Delta_{\mathbb{S}^2}\right)\Psi = 0\,, \tag{7}$$

which is regular under compactification.

By performing this hyperboloidal compactification, we foliate spacetime into hypersurfaces that are spacelike everywhere and extend from the origin to future null infinity. They are called hyperboloidal slices and are represented in Fig. 1 for Minkowski spacetime.

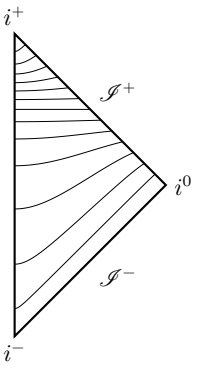

FIG. 1: Penrose diagram of Minkowski spacetime foliated along hyperboloidal slices.

3. THE GBU MODEL

The good-bad-ugly (GBU) model is a model of GR. It represents the three types of field equations that appear in the EFE, and consists of the following equations

$$\Box g \simeq 0\,, \tag{8a}$$
$$\Box b \simeq (\nabla_T g)^2\,, \tag{8b}$$
$$\Box u \simeq \frac{2}{R}\nabla_T u\,, \tag{8c}$$

where g stands for *good*, b for *bad* and u for *ugly*. In this work, we will not be interested in *bad* fields, since we are focusing on linearized theory where non-linear equations like (8b) do not appear.

Good fields decay like a solution to the wave equation, whereas *ugly* fields decay faster near future null infinity. A careful discussion of the asymptotics of these fields can be found in [5]. By modeling the linearized EFE as *good* and *ugly* equations, we can understand the rate of decay of the fields, which will in turn help us understand how to rescale them such that they attain a non-vanishing finite limit at future null infinity. The propagating degrees of freedom manifest in the curvature, h_+ and $h_\times$, will be modeled as *goods*, since they are the quantities we measure on Earth (i.e. they should not decay as fast as all the other quantities), whereas the other eight independent metric components will be modeled as *uglies*.

4. GEOMETRIC SETUP

4.1. Geometric quantities

We define the outgoing and incoming null vectors, respectively, as

$$\xi^\mu = \partial_T^\mu + C_+^R\partial_R^\mu\,, \tag{9}$$
$$\underline{\xi}^\mu = \partial_T^\mu + C_-^R\partial_R^\mu\,, \tag{10}$$

where the quantities $C^R_\pm$ can be interpreted as coordinate light speeds. Derivatives along the outgoing null direction ξ^μ and angular derivatives are called good derivatives, since they improve the fall-off of the fields they are applied to. On the other hand, derivatives along the ingoing null direction are called bad derivatives, since they do not change the rate of decay of the fields.

The co-vectors are defined as

$$\eta_\mu = -C^R_+\nabla_\mu T + \nabla_\mu R - C^+_A\nabla_\mu\theta^A\,, \tag{11}$$

$$\underline{\eta}_\mu = C^R_-\nabla_\mu T - \nabla_\mu R + C^-_A\nabla_\mu\theta^A\,, \tag{12}$$

where $A = \theta, \phi$.

The inverse metric can be expressed as

$$g^{\mu\nu} = -\frac{2e^{-\varphi}}{\tau}\xi^{(\mu}\underline{\xi}^{\nu)} + \not{g}^{\mu\nu}\,, \tag{13}$$

where $\tau = C^R_+ - C^R_-$. The first term of Eq. (13) encapsulates the radial causal structure of spacetime, and φ is related to its determinant. The last term, $\not{g}^{\mu\nu}$, captures the physics along the directions orthogonal to the radial null directions. It is the inverse of a 4×4 symmetric matrix whose only non-vanishing components are the angular ones

$$\not{g}_{\mu\nu} = \mathring{R}^2\, q_{\mu\nu}\,, \tag{14}$$

where we define the 2-metric $q_{\mu\nu}$ as

$$q_{\mu\nu} = \begin{pmatrix} 0 & 0 & 0 & 0 \\ 0 & 0 & 0 & 0 \\ 0 & 0 & e^{h_+}\cosh h_\times & \sin\theta\sinh h_\times \\ 0 & 0 & \sin\theta\sinh h_\times & e^{-h_+}\cosh h_\times \sin\theta^2 \end{pmatrix}. \tag{15}$$

$\mathring{R}$, h_+ and $h_\times$ are the three independent quantities contained in $\not{g}_{\mu\nu}$. h_+ and $h_\times$ are the propagating degrees of freedom of the GWs manifest in the curvature, i.e. the quantities we measure on Earth, and $\mathring{R}$ is related to the determinant of $\not{g}_{\mu\nu}$.

To determine the inverse of the 2-metric, we use the following *ansatz*

$$q^{\mu\nu} = \begin{pmatrix} f1 & f2 & f5 & f6 \\ f3 & f4 & f7 & f8 \\ f5 & f7 & e^{-h_+}\cosh h_\times & -\csc\theta\sinh h_\times \\ f6 & f8 & -\csc\theta\sinh h_\times & e^{h_+}\cosh h_\times \csc\theta^2 \end{pmatrix}, \tag{16}$$

where the f's are arbitrary functions of the coordinates (T, R, θ, ϕ).

We use the fact that η_μ and $\underline{\eta}_\mu$ are null co-vectors, and therefore they are orthogonal to $\not{g}^{\mu\nu}$, i.e.

$$\not{g}^{\mu\nu}\eta_\mu = 0 \qquad \text{and} \qquad \not{g}^{\mu\nu}\underline{\eta}_\mu = 0\,, \tag{17}$$

to determine the f functions, thus obtaining the components of $\not{g}^{\mu\nu}$. Their explicit lengthy expressions are omitted here for the sake of clarity. With this, we can at last write both the metric and its inverse, which suffice to define all the geometric quantities, such as the Christoffel symbols and the Riemann tensor.

4.2. Linearization

To linearize, we take Minkowski spacetime as the background. An interesting follow-up calculation would be to linearize around different backgrounds, which was not done in this project due to time constraints. We perform the linearization by expressing the variables as the value they take in flat spacetime plus a small, perturbative term

$$C_+ = 1 + \epsilon\,\delta C^R_+\,, \tag{18a}$$

$$C_- = -1 + \epsilon\,\delta C^R_-\,, \tag{18b}$$

$$C^\pm_A = 0 + \epsilon\,\delta C^\pm_A\,, \tag{18c}$$

$$\varphi = 0 + \epsilon\,\delta\varphi\,, \tag{18d}$$

$$\mathring{R} = R + \epsilon\,\delta\mathring{R}\,, \tag{18e}$$

$$h_{+,\times} = 0 + \epsilon\,\delta h_{+,\times}\,. \tag{18f}$$

By substituting these in the metric, and linearizing in the usual way,

$$h_{\mu\nu} = \lim_{\epsilon\to 0}\partial_\epsilon g_{\mu\nu}\,, \tag{19}$$

one obtains the linearized metric. We can also define the linearized Ricci tensor in the same way

$$\tilde{R}_{\mu\nu} = \lim_{\epsilon\to 0}\partial_\epsilon R_{\mu\nu}\,. \tag{20}$$

A useful quantity to define when one works in the linearized theory is $\bar{h}_{\mu\nu}$,

$$\bar{h}_{\mu\nu} = h_{\mu\nu} - \frac{1}{2}\eta_{\mu\nu}h\,. \tag{21}$$

Its components can be written in terms of the variables $\delta C_\pm$, $\delta C^\pm_A$, $\delta\varphi$, $\delta\mathring{R}^{-1}$, and $\delta h_{+,\times}$. Hence, the evolution equations for these variables contain all the physical information of the system.

The background quantities take their flat spacetime value and are denoted with a dot on top. For instance, the flat background metric in spherical coordinates is $\dot{g}_{\mu\nu} = \mathrm{diag}(-1, 1, R^2, R^2\sin^2\theta)$.

5. REGULARIZATION AT THE ORIGIN AND FUTURE NULL INFINITY

In spherical coordinates, the equations contain terms that diverge with $\mathcal{O}(R^{-2})$ and $\mathcal{O}(\sin^{-2}\theta)$. Choosing as evolved variables a proper rescaling of the tensorial quantities, all code variables remain finite [6]. Furthermore, evolved variables need to be sufficiently smooth functions (at least C^2). Let us obtain the conditions that make the evolved variables satisfy these requirements.

Consider a generic 2-tensor $g_{\mu\nu}$ in Cartesian coordinates which is well-defined at the origin. We wish to perform a coordinate transformation – to spherical polar coordinates – in such a way that it remains well-defined near the origin. In the new coordinates,

the components of the tensor $g_{\mu'\nu'}$ can be computed in the following way

$$g_{\mu'\nu'} = J^{\mu}{}_{\mu'} g_{\mu\nu} J_{\nu'}{}^{\nu}\,, \tag{22}$$

where $J_{\mu'}{}^{\mu}$ stands for the Jacobian matrix.

We expand the tensor components in terms of the coordinates and check the conditions that ensure the components and their derivatives are well-defined at the origin, i.e. they take the same limit independently of the direction we approach the origin from. We conclude that a generic tensor can be expressed near the origin in spherical polar coordinates as

$$\begin{aligned} g_{\mu'\nu'} = \mathrm{diag}(&g_{TT}, g^0_{RR} + \frac{R^2}{2}\partial_r^2 g_{RR}, && (23)\\ &g^0_{RR} R^2 + \frac{R^4}{2}\partial_r^2 g_{\theta\theta}, && (24)\\ &g^0_{RR} R^2 \sin^2\theta + \frac{R^4 \sin^2\theta}{2}\partial_r^2 g_{\theta\theta})\,, && (25) \end{aligned}$$

where the derivatives are computed at the origin.

In other words, g_{TT} and g_{RR} are even functions of R and the following conditions must be satisfied

$$\begin{aligned} &g_{TR} = \mathcal{O}(R)\,, && g_{T\theta} = \mathcal{O}(R^2)\,,\\ &g_{T\phi} = \mathcal{O}(R^2)\,, && g_{RR} - \tfrac{g_{\theta\theta}}{R^2} = \mathcal{O}(R^2)\,,\\ &g_{\theta\phi} = \mathcal{O}(R^3)\,, && g_{RR} - \tfrac{g_{\phi\phi}}{R^2\sin^2\theta} = \mathcal{O}(R^2)\,,\\ &g_{R\theta} = \mathcal{O}(R^3)\,, && g_{R\phi} = \mathcal{O}(R^3)\,. \end{aligned} \tag{26}$$

The regularity conditions in terms of our variables imply that, at the origin, the following conditions must be satisfied

$$\begin{aligned} &\tfrac{\delta\dot{R}}{R} = \mathcal{O}(1) + \mathcal{O}(R^2)\,, && \partial_R \delta C^R_- = \partial_R \delta C^R_+\,,\\ &\delta C^R_+ + \delta C^R_- = \mathcal{O}(R)\,, && \delta C^-_\theta - \delta C^+_\theta = \mathcal{O}(R)\,,\\ &\delta C^-_\phi - \delta C^+_\phi = \mathcal{O}(R)\,, && \delta C^-_\theta + \delta C^+_\theta = \mathcal{O}(R^2)\,,\\ &\delta h_+ = \mathcal{O}(R^2)\,, && \delta C^-_\phi + \delta C^+_\phi = \mathcal{O}(R^2)\,,\\ &\delta h_\times = \mathcal{O}(R)\,, \end{aligned} \tag{27}$$

$$\delta\varphi + \frac{1}{2}(\delta C^R_- - \delta C^R_+) = \mathcal{O}(1) + \mathcal{O}(R^2)\,.$$

We follow the approach taken in [7] and [8] to regularize the evolution equations at future null infinity. To do so, we come back to the GBU model. Since we are only interested in *good* and *ugly* fields – recall that the *bad* equation had a non-linear term and thus it does not appear in the linearized equations –, we will focus only on the GU equations

$$\Box g = S_g(T, R, \theta, \phi)\,, \tag{28a}$$

$$\Box u - \frac{2}{\chi(R)}\nabla_T u = S_u(T, R, \theta, \phi)\,, \tag{28b}$$

with

$$\lim_{R\to\infty} \chi(R) = R\,. \tag{29}$$

For the purpose of this section, we take $\chi(R) = R$ since we are only interested in the asymptotic behavior. For the numerical implementation, it will be important to redefine $\chi(R)$ as an even function so that *ugly* fields are, like a solution to the wave equation, even. However, in the context of the asymptotic regime, the parity of the fields can be ignored. Furthermore, we consider source terms S_g and S_u. We assume that the source terms decay much faster than the fields – at least like $\mathcal{O}(R^{-3})$ –, so that, in the asymptotic regime, the equations approach Eqs. (8a) and (8c), respectively.

In order to allow for implementations with pseudo-spectral methods, we perform a first-order reduction, i.e. we define new evolved variables as a combination of first-order derivatives of the fields such that we get an equivalent system of equations with only first-order derivatives. For *good* fields, we define

$$g^+ := \partial_T g + \partial_R g\,, \tag{30a}$$

$$g^- := \partial_T g - \partial_R g\,, \tag{30b}$$

$$g_A := \partial_A g\,, \tag{30c}$$

where g^+ and g^- are simply the good and bad derivatives of g, respectively, and similarly for *ugly* fields.

Hence, Eq. (28a) can be expressed as the system of equations

$$\partial_T g = \frac{1}{2}(g^+ + g^-)\,, \tag{31a}$$

$$\partial_T g^+ = -S_g + \frac{1}{R}(g^+ - g^-) + \frac{1}{R^2}\not{D}^A g_A + \partial_R g^+\,, \tag{31b}$$

$$\partial_T g^- = -S_g + \frac{1}{R}(g^+ - g^-) + \frac{1}{R^2}\not{D}^A g_A - \partial_R g^-\,, \tag{31c}$$

$$\partial_T g_A = \frac{1}{2}\partial_A(g^+ + g^-)\,, \tag{31d}$$

where

$$\not{D}^A \psi_A = \frac{1}{\sqrt{\not{g}}}\partial_A(\sqrt{\not{g}}\not{g}^{AB}\psi_B) \tag{32}$$

is the divergence on the 2-sphere, and Eq. (28b) can be expressed as

$$\partial_T u = \frac{1}{2}(u^+ + u^-)\,, \tag{33a}$$

$$\partial_T u^+ = -S_u - \frac{2}{R}u^- + \frac{1}{R^2}\not{D}^A u_A + \partial_R u^+\,, \tag{33b}$$

$$\partial_T u^- = -S_u - \frac{2}{R}u^- + \frac{1}{R^2}\not{D}^A u_A - \partial_R u^-\,, \tag{33c}$$

$$\partial_T u_A = \frac{1}{2}\partial_A(u^+ + u^-)\,. \tag{33d}$$

After performing the hyperboloidal compactification, we get

$$\partial_t g = \frac{1}{2}(g^+ + g^-)\,, \tag{34a}$$

$$\partial_t g^+ = -\frac{S_g}{1+H'} + \frac{g^+ - g^-}{R(1+H')} + \frac{\not{D}^A g_A}{R^2(1+H')} + \frac{\partial_r g^+}{R'(1+H')}\,, \tag{34b}$$

$$\partial_t g^- = \frac{S_g}{-1+H'} - \frac{g^+ - g^-}{R(-1+H')} - \frac{\not{D}^A g_A}{R^2(-1+H')} + \frac{\partial_r g^-}{R'(-1+H')}\,, \tag{34c}$$

$$\partial_t g_A = \frac{1}{2}\partial_A(g^+ + g^-)\,, \tag{34d}$$

and

$$\partial_t u = \frac{1}{2}(u^+ + u^-)\,, \tag{35a}$$

$$\partial_t u^+ = -\frac{S_u}{1+H'} - \frac{2u^-}{R(1+H')} + \frac{\not{D}^A u_A}{R^2(1+H')} + \frac{\partial_r u^+}{R'(1+H')}\,, \tag{35b}$$

$$\partial_t u^- = \frac{S_u}{-1+H'} + \frac{2u^-}{R(-1+H')} - \frac{\not{D}^A u_A}{R^2(-1+H')} + \frac{\partial_r u^-}{R'(-1+H')}\,, \tag{35c}$$

$$\partial_t u_A = \frac{1}{2}\partial_A(u^+ + u^-)\,, \tag{35d}$$

where $H \equiv H(R)$ is the height function defined in section 2. For these equations to be numerically regular at future null infinity, the coefficients must be at most $\mathcal{O}(1)$. We demand that $H' = 1 - R'^{-1}$, and choose R such that $R' \sim \mathcal{O}(R^2)$. Note that the source terms, S_g and S_u, must decay at least like $\mathcal{O}(R^{-2})$ in order for the first term on the RHS to be regular. The coefficient in the second term of the RHS of Eqs. (34d) and (35d) is $\mathcal{O}(R)$ and therefore these equations are not regular at $\mathscr{I}^+$. We can redefine our evolved variables to include such diverging terms. Therefore, we introduce the rescaled fields

$$G = \chi(R) g\,, \tag{36a}$$

$$G^+ = \chi(R)(\chi(R) g)^+\,, \tag{36b}$$

$$G^- = \chi(R) g^-\,, \tag{36c}$$

$$G_A = \chi(R)\tilde{\partial}_A g\,, \tag{36d}$$

where $\tilde{\partial}_A = (\partial_\theta, \frac{1}{\sin(\theta)}\partial_\phi)^T$. Analogously, we introduce rescaled fields for u. In the asymptotic regime, the equations become

$$\partial_t G \simeq \frac{1}{2}G^- - \frac{1}{2R}G + \frac{1}{2R}G^+\,, \tag{37a}$$

$$\partial_t G^+ \simeq -c^r_- G^+ - \mathcal{A}^- \not{D}^A G_A + S_{G^+} \tag{37b}$$

$$\partial_t G^- \simeq -c^r_- \partial_r G^- + \mathcal{A}^+ \not{D}^A G_A + S_{G^-} \tag{37c}$$

$$\partial_t G_A \simeq \frac{\tilde{\partial}_A G^+}{2R} + \frac{1}{2}\tilde{\partial}_A G^- - \frac{G_A}{2R}\,, \tag{37d}$$

and

$$\partial_t U \simeq \frac{1}{2}U^- - \frac{1}{2R}U + \frac{1}{2R}U^+\,, \tag{38a}$$

$$\partial_t U^+ \simeq -c^r_- U^+ - \mathcal{A}^- \not{D}^A U_A + S_{U^+}, \tag{38b}$$

$$\partial_t U^- \simeq -c^r_+ \partial_r U^- + \mathcal{A}^+ \not{D}^A U_A + S_{U^-}\,, \tag{38c}$$

$$\partial_t U_A \simeq \frac{\tilde{\partial}_A U^+}{2R} + \frac{1}{2}\tilde{\partial}_A U^- - \frac{U_A}{2R}\,, \tag{38d}$$

where we have introduced the following quantities

$$\alpha_+ = 1\,, \tag{39a}$$

$$\alpha_- = \chi\,, \tag{39b}$$

$$c^r_\pm = \frac{\pm 1}{(1 \mp H')R'}\,, \tag{39c}$$

$$\mathcal{A}^\pm = \frac{R'}{R}\alpha_\pm c^r_\pm\,. \tag{39d}$$

The lower-order terms are contained in S_{G^+}, S_{G^-}, S_{U^+}, S_{U^-}.

Besides making the equations numerically more regular at $\mathscr{I}^+$, this choice of evolved variables is appropriate since it allows us to extract the radiation fields directly.

6. EQUATIONS OF MOTION

Recall the ten independent metric components $\delta C_\pm$, $\delta C^\pm_A$, $\delta\varphi$, $\delta\mathring{R}^{-1}$, and $\delta h_{+,\times}$, whose evolution accommodates the physical information of the system. Two of these – $\delta h_{+,\times}$ – behave like a solution to the wave equation. Hence, they will be modeled as *goods*, whereas the other eight fields, which decay faster asymptotically, will be modeled as *uglies*. We are thus looking to have two equations of the form of Eq. (28a) and eight of the form of Eq. (28b).

Alternatively, since we have that $T^a = \frac{1}{2}(\xi^a + \underset{\sim}{\xi}^a)$, the *ugly* equation can be expressed in the form

$$\Box_1 u := \Box u - R^{-1}\nabla_{\underset{\sim}{\xi}} u = \tilde{S}_u\,, \tag{40}$$

where $\tilde{S}_u = S_u + \nabla_{\underset{\sim}{\xi}} u$.

The appropriate rate of decay of the fields can be imposed, i.e. we can force the eight *ugly* equations to have the form of Eq. (40), through gauge fixing and constraint addition.

6.1. Generalized Harmonic Gauge

In this work, we impose a generalization of the harmonic gauge – the Generalized Harmonic Gauge

(GHG) – that not only leads to well-posed equations but also allows us to impose the rate of decay of the fields such that they attain a non-vanishing finite limit at future null infinity.

In GHG, instead of setting the divergence of $\bar{h}_{\mu\nu}$ to zero, we set it to some arbitrary functions of the coordinates

$$\nabla^\nu \bar{h}_{\mu\nu} + F_\mu = 0\,. \tag{41}$$

These functions can be used to impose the rate of decay of four of the fields. We also define a harmonic constraint equal to the quantity above,

$$Z_\mu \equiv \nabla^\nu \bar{h}_{\mu\nu} + F_\mu\,, \tag{42}$$

which is used to impose conditions on four other fields.

We define a new linearized Ricci tensor

$$\delta\mathcal{R}_{\mu\nu} \equiv \delta R_{\mu\nu} - \nabla_{(\mu} Z_{\nu)} + W_{\mu\nu}\,, \tag{43}$$

where the second term cancels the terms in the linearized Ricci tensor that are not the wave operator and $W_{\mu\nu}$ is a sparse matrix with components that depend only on the harmonic constraint. The evolution equations are obtained by making the appropriate contractions with $\delta\mathcal{R}_{\mu\nu}$. For instance, the equation of motion (EOM) for δC^R_+ is obtained by

$$\xi^\mu\xi^\nu \delta\mathcal{R}_{\mu\nu} = 0\,. \tag{44}$$

The remaining seven *ugly* equations are obtained by making the following contractions: $\xi^\mu \mathcal{R}_{\mu A}$, $\not{g}^{\mu\nu}\mathcal{R}_{\mu\nu}$, $\xi^\mu\xi^\nu\mathcal{R}_{\mu\nu}$, $\xi^\mu \mathcal{R}_{\mu A}$, $\xi^\mu\xi^\nu\mathcal{R}_{\mu\nu}$.

Recall that we can choose the gauge source functions to make four fields be modeled as *uglies*, namely δC^R_-, δC^-_A, and $\delta\varphi$. The choice that satisfies this requirement is

$$F_\xi = \frac{\delta\varphi}{R}\,, \qquad F_{\xi} = -\frac{\delta C^R_-}{R}\,, \qquad F_A = \delta C^+_A\,. \tag{45}$$

With this choice, the equations yield

$$\Box_1 \delta C^R_+ = 2R^{-1}\nabla_\xi(R\delta\mathring{R}^{-1} + \delta\varphi) + \not{D}^A \delta C^+_A\,, \tag{46a}$$

$$\Box_1 \delta C^+_A = -\frac{2}{R^2}\nabla^B \hat{h}_{AB} + \frac{2\delta C^+_A}{R^2} + \frac{4\partial_A \delta\mathring{R}^{-1}}{R} \tag{46b}$$

$$+ \frac{4\partial_A\delta\varphi}{R^2} - \frac{2\partial_A \delta C^R_+}{R^2}\,, \tag{46c}$$

$$\Box_1 \delta\mathring{R}^{-1} = \frac{2\delta\varphi}{R^3} + \frac{\delta C^R_-}{2R^3} - \frac{\nabla_\xi \delta\mathring{R}^{-1}}{R} + \frac{\delta C^R_-}{2R^3} \tag{46d}$$

$$- \frac{\delta C^R_+}{2R^3} + \not{D}^A \delta C^-_A\,, \tag{46e}$$

$$\Box_1 \delta C^R_- = \frac{3\delta C^R_-}{R^2} + \frac{2\delta\varphi}{R^2} + \frac{4\delta\mathring{R}^{-1}}{R} - 2\not{D}^A\delta C^-_A\,, \tag{46f}$$

$$\Box_1 \delta C^-_A = \frac{3\partial_A \delta C^R_-}{R^2} - \frac{\delta C^-_A}{R^2} - \frac{\delta C^+_A}{R^2} + \frac{4\partial_A\delta\mathring{R}^{-1}}{R} \tag{46g}$$

$$- \frac{2\nabla_\xi \delta C^-_A}{R} - \frac{1}{R} Z_A\,, \tag{46h}$$

$$\Box_1 \delta\varphi = \frac{2\delta\varphi}{R^2} + \frac{4\delta\mathring{R}^{-1}}{R} - \frac{1}{2}\nabla_\xi \frac{\delta C^R_-}{R} \tag{46i}$$

$$+ \frac{\delta C^R_- - \delta C^R_+}{R^2} + \not{D}^A(\delta C^+_A + \delta C^-_A)\,. \tag{46j}$$

The *good* equations are straightforward to obtain. We define the projected linearized metric on the background 2-sphere

$$\hat{h}_{\mu\nu} = \perp_{\mu\nu}{}^{\alpha\beta} h_{\alpha\beta}\,, \tag{47}$$

where the projection operator is given by

$$\perp_{\mu\nu}{}^{\alpha\beta} = (\dot{\not{g}}_{(\mu}{}^{\alpha}\dot{\not{g}}_{\nu)}{}^{\beta} - \frac{1}{2}\dot{\not{g}}_{\mu\nu}\dot{\not{g}}^{\alpha\beta})\,, \tag{48}$$

and applying the D'Alembert operator we get

$$\Box\hat{h}_{AB} = 2\perp^{ab}_{AB} \not{\nabla}_{(a|}\delta C^-_{|b)} + M_{AB}\not{\nabla}_a(\delta C^{R,a}_+ + \delta C^{R,a}_-)\,, \tag{49}$$

where

$$M_{AB} = \begin{pmatrix} 1 & 0 \\ 0 & -1 \end{pmatrix}\,. \tag{50}$$

These equations have the form we expected them to have, (40) for eight of the fields and (28a) for the propagating degrees of freedom, with right-hand sides (RHSs) $\sim \mathcal{O}(R^{-3})$. This proves that the linearized Einstein equations can indeed be modeled by the GU equations.

6.2. Transverse-Traceless gauge

Let us now compare our gauge with the usual Transverse-Traceless (TT) gauge. In TT gauge we have that

$$h^{TT} = 0\,, \qquad \bar{h}^{TT}_{0\mu} = 0\,. \tag{51}$$

These conditions must be satisfied by the initial data, at $t = 0$, and later. Thus, in terms of our variables, the conditions above translate to

$$\begin{gathered} \delta C^R_+ = -\delta C^R_-\,,\ \delta C^+_A = \delta C^-_A\,, \\ \delta\mathring{R}^{-1} = \tfrac{\delta C^R_-}{2R}\,, \quad \delta\varphi = \delta C^R_-\,, \end{gathered} \tag{52}$$

and a similar relation for the time derivatives of the fields. By considering these relations, and choosing the gauge source functions to be zero, we see that equations for the dependent variables turn out to be the same as the EOMs for the independent variables, indicating that if we impose TT gauge for the initial data, it gets propagated.

7. NUMERICAL SIMULATIONS

For the numerical implementation, we use NRPy+, which is a collection of python scripts that generates optimized code in C, and is mostly used for solving problems in Numerical Relativity (NR). The first paper on NRPy+ was released on December 2017 [9]. This package comes with several helpful tutorials. For our problem, in particular, the most relevant tutorial is *Tutorial-Start_to_Finish-ScalarWaveCurvilinear.ipynb*, which allows us to solve the scalar wave equation in spherical coordinates. Taking advantage of this code, we modified it to solve our equations in the hyperboloidal setting.

7.1. Implemented equations

In the numerical implementation, we choose

$$R(r) = \frac{r}{1-r}\,, \tag{53}$$

so that $\mathscr{I}^+$ corresponds to the point at $r = 1$, and set the height function to

$$H(r) = R(r) - r\,. \tag{54}$$

For the rescaling function $\chi(R)$, we choose

$$\chi(R) = \sqrt{1+R^2}\,, \tag{55}$$

so that it is an even function that does not vanish at the origin and approaches R asymptotically. Therefore, in the asymptotic limit we recover Eqs. (37) and (38).

We set the source terms S_g and S_u to zero. In the future, we could expand this work by considering non-vanishing source terms.

The implemented equations read

$$\partial_t G = \frac{1}{2}G^- - \frac{R}{2\chi^2}G + \frac{1}{2\chi}G^+\,, \tag{56a}$$

$$\partial_t G^+ = -c^r_- G^+ - \mathcal{A}^- \not{D}^A G_A + S_{G^+} \tag{56b}$$

$$\partial_t G^- = -c^r_- \partial_r G^- + \mathcal{A}^+ \not{D}^A G_A + S_{G^-} \tag{56c}$$

$$\partial_t G_A = \frac{\tilde{\partial}_A G^+}{2\chi} + \frac{1}{2}\tilde{\partial}_A G^- - \frac{R}{2\chi^2}G_A\,, \tag{56d}$$

$$\partial_t U = \frac{1}{2}U^- - \frac{R}{2\chi^2}U + \frac{1}{2\chi}U^+\,, \tag{56e}$$

$$\partial_t U^+ = -c^r_- U^+ - \mathcal{A}^- \not{D}^A U_A + S_{U^+}, \tag{56f}$$

$$\partial_t U^- = -c^r_+ \partial_r U^- + \mathcal{A}^+ \not{D}^A U_A + S_{U^-}\,, \tag{56g}$$

$$\partial_t U_A = \frac{\tilde{\partial}_A U^+}{2\chi} + \frac{1}{2}\tilde{\partial}_A U^- - \frac{R}{2\chi^2}U_A\,, \tag{56h}$$

where we use the same notation as in section .

The method of lines is employed for time integration and is performed with a fourth-order accurate Runge-Kutta scheme. Second-order centered finite differences are used to approximate spatial derivatives. We add Kreiss-Oliger dissipation [10] to our equations, which consists of adding a term to the RHS of the form

$$\sigma(\Delta x)^3 D_+^2 D_-^2 \psi/16\,, \tag{57}$$

where σ is the dissipation strength, Δx is the grid spacing, $D_\pm$ the standard forward and backward differencing operators and ψ stands for a field. For our simulations in axial symmetry, we used dissipation strength $\sigma = 0.2$.

We work with a staggered grid, i.e. there are no grid points exactly at the origin and at $\mathscr{I}^+$, but they get closer as the resolution is increased.

7.2. Boundary Conditions

Our numerical domain satisfies

$$r \in [0,1]\,, \quad \theta \in [0,\pi]\,, \quad \phi \in [-\pi,\pi]\,. \tag{58a}$$

In spherical coordinates, there are two types of numerical boundaries – inner and outer. To define the boundary conditions, we introduce points that lay beyond the domains defined above and that serve only for numerical purposes, not having any physical meaning – we call them ghost points. These points are distributed into ghost zones, which are like layers. We use two ghost zones, meaning that we extend the grid in every direction by two points. Due to the hyperboloidal compactification we performed, no outer boundary conditions are needed. However, we do need to fill in the ghost points, which we do via extrapolation.

Most of the quantities we consider are even, because, since g is a solution to the wave equation, it is even in R as long as we start with an even function of R as initial data. Any derivative that does not involve the radial coordinate is therefore also even, for instance, $\partial_T g$ and $\partial_A g$. Thus, as long as we choose $\chi(R)$ to be an even function of R – which we have – G and G_θ are even. Notice that, for our choice of $R(r)$, (53), an even function of R is also an even function of r. An even function of r, ψ, satisfies the inner boundary conditions

$$\psi(r,\theta,\pm\pi\pm\phi) = \psi(r,\theta,\pm\pi\mp\phi)\,, \tag{59a}$$

$$\psi(r,-\theta,\phi) = \psi(r,|-\theta|,\phi\pm\pi)\,, \tag{59b}$$

$$\psi(r,\pi+\theta,\phi) = \psi(r,\pi-\theta,\phi\pm\pi)\,, \tag{59c}$$

$$\psi(-r,\theta,\phi) = \psi(r,\pi-\theta,\phi\pm\pi)\,, \tag{59d}$$

where in the last three relations the sign in $\phi \pm \pi$ is chosen such that the resulting points lie inside the domain.

However, the parity of the characteristic fields is not as straightforward since they include radial derivatives of the fields. But since $\partial_T g$ is even, from definition of the characteristic fields, we have that $g^+(-R) - \partial_R g(-R) = g^-(R) + \partial_R g(R)$. Writing this in terms of the rescaled fields and in hyperboloidal coordinates,

we obtain the parity conditions for G^+ and G^-, which are neither even nor odd,

$$G^+(-r) = \chi(R(r))G^-(r) - \chi'(R(r))G(r)\,, \quad (60a)$$
$$G^-(-r) = \frac{G^+(r)}{\chi(R(r))} - \frac{\chi'(R(r))G(r)}{\chi(R(r))}\,, \quad (60b)$$

and similarly for U.

7.3. Numerical treatment of the origin

Our equations have formally singular terms of the form $\frac{2}{r}\psi$. We solve this by applying Evan's method [11], as discussed in [8, 12], which consists of defining a new differencing operator that includes these diverging terms, $\tilde{D}$. Thus, the system

$$\partial_t\psi = \partial_r\pi\,, \quad (61a)$$
$$\partial_t\pi = \partial_r\psi + \frac{2}{r}\psi\,, \quad (61b)$$

turns into

$$\partial_t\psi = \Delta r^{-1} D\pi\,, \quad (62a)$$
$$\partial_t\pi = \Delta r^{-1}\tilde{D}\psi\,, \quad (62b)$$

where the differencing operators are computed by

$$\tilde{D}\psi = 3\frac{r_{i+1}^2\psi_{i+1} - r_{i-1}^2\psi_{i-1}}{r_{i+1}^3 - r_{i-1}^3}\,, \quad (63a)$$
$$D\pi = \frac{\pi_{i+1} - \pi_{i-1}}{2}\,. \quad (63b)$$

In this way, we avoid diverging terms on the RHSs.

7.4. Initial Data

Initial data must be smooth functions everywhere. We consider the spherical harmonics,

$$\varphi = \sum_{l=0}^{\infty}\sum_{m=-l}^{m=l}\varphi_{lm}(t,r)Y_{lm}(\theta^A)\,, \quad (64)$$

where φ_{lm} is given by

$$\varphi_{lm} = \sum_{k=0}^{l}\frac{(k+l)!}{2^k k!(l-k)!}\frac{1}{r^{k+1}}[F^{l-k}(u) - (-1)^{l-k}F^{l-k}(v)]\,, \quad (65)$$

with $u = t - r$ the retarded time and $v = t + r$ the advanced time.

We make a similar choice for the initial data of G and U, $t = 0$, in axial symmetry as in [13], $\varphi_{20}Y_{20}$, where

$$Y_{20} = \frac{1}{4}\sqrt{\frac{5}{\pi}}(3\cos^2\theta - 1)\,, \quad (66)$$

and we take

$$F(r) = e^{-(r-1/4)^2}\,. \quad (67)$$

The initial data for the other fields are computed straightforwardly by taking the appropriate derivatives and rescalings, in accordance with their definition (36).

7.5. Results

In the following, we present the numerical results from the implementation. Since the simulation was done in axial symmetry, G_ϕ and U_ϕ are zero everywhere. Thus, they are omitted from this discussion.

The basic dynamics of the evolution of the G_θ and U_θ fields is represented in Fig. 2. We present the results for these fields in particular, since they constitute a new contribution – as so far, only the spherically symmetric case had been done – namely, the evolution of *ugly* fields in axial symmetry in hyperboloidal coordinates in first-order in space (i.e, with only first-order spatial derivatives). We see that the *ugly* field, U_θ, decays must faster than the *good* one, and is always zero at $\mathscr{I}^+$, as expected. *Ugly* fields decay faster than a solution to the wave equation, i.e. at least like $\mathcal{O}(R^{-3})$. Consequently, even when rescaled by $\chi(R)$ they decay fast enough to vanish at $\mathscr{I}^+$.

To check convergence the code was first run with 80 grid points in r, 16 in θ and 4 in ϕ, and then the resolution in r and θ was iteratively increased by a factor of $p = 1.5$ in the two following runs.

To compute the convergence factor, we considered the energy norm as defined in [14]

$$E(t) = \int_\Sigma \varepsilon dr d\Omega\,, \quad (68)$$

with

$$\varepsilon = \frac{1}{2}\left[\left(\frac{2R'-1}{2R'}\right)(\psi^+)^2 + \left(\frac{1}{2R'}\right)(\psi^-)^2 + \frac{1}{R^2}\psi_\theta^2 + \frac{1}{R^2\sin\theta}\psi_\phi^2\right]R^2R'\,, \quad (69)$$

where ψ stands for the fields (*goods* and *uglies*) before being rescaled (see (30a)). The convergence factor of the state-vector $(G, G^+, G^-, G^\theta, U, U^+, U^-, U^\theta)$ defined with the norm (69) is plotted in Fig. 3. We observe that it is roughly 2, as expected for a second-order finite difference approximation (chosen in this experiment), suggesting a successful result.

We performed pointwise convergence at $\mathscr{I}^+$ to further ensure the correctness of the results. To do that, we used a fourth-order extrapolation of the *good* fields at future null infinity (recall that the *ugly* fields all vanish at $\mathscr{I}^+$, thus this analysis is pointless for those fields). Then we computed the differences between high and medium resolutions and between medium and low. The latter was rescaled by a factor of 1.5^2, and the result is plotted in Fig. 4. We can see that the rescaled differences align almost perfectly on top of each other, indicating convergence at $\mathscr{I}^+$.

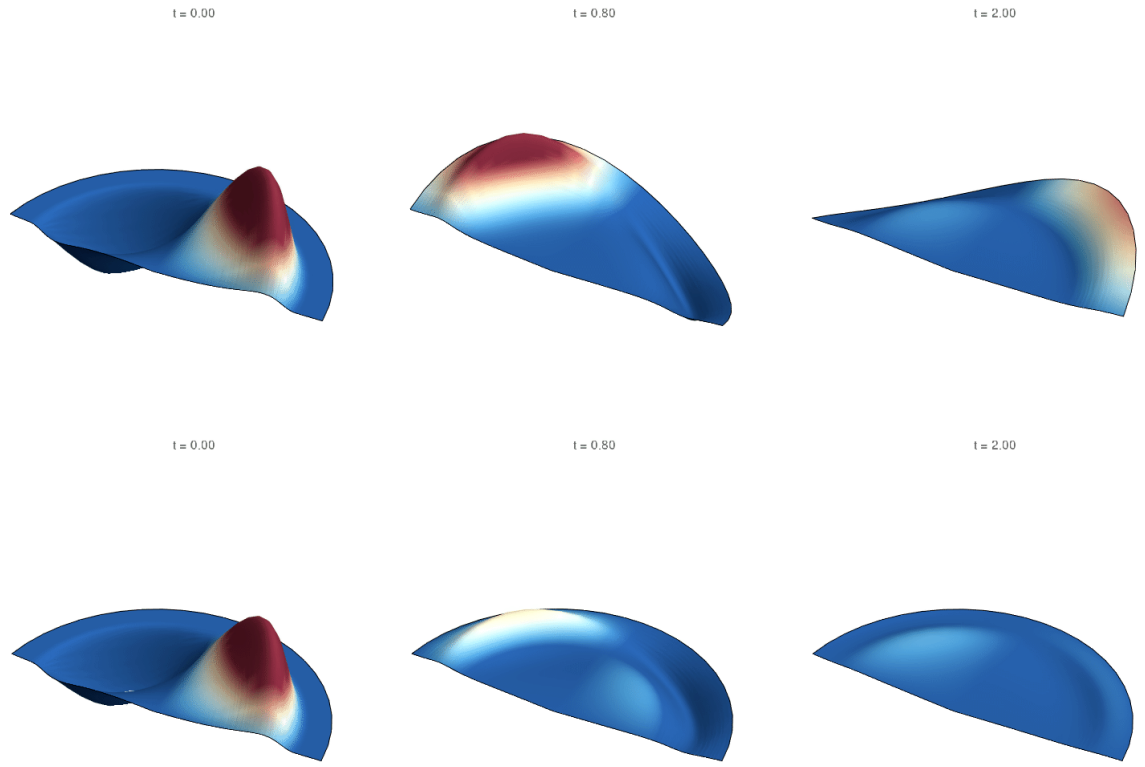

FIG. 2: Dynamics of the evolution of the G_θ (on top) and U_θ (on the bottom panel) fields in axial symmetry starting with initial data according to Sec. 7.4. The evolution depicted here was performed with 120 grid points in the radial coordinate, 24 grid points in θ, and 4 points in ϕ. Although we are taking an axially symmetric expression for the initial data, we use 4 points in ϕ. Even though we are evolving axially symmetric data, four points in ϕ are needed for the boundary conditions, which have two ghost zones. As expected, the *ugly* fields decay must faster than the *goods*, and are always zero at future null infinity.

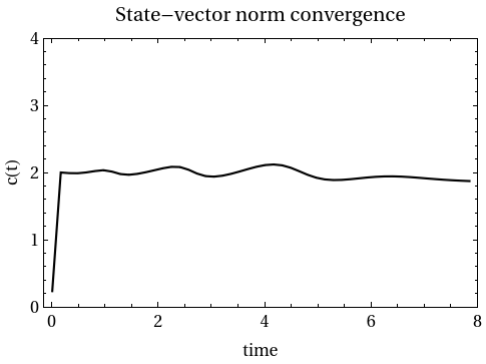

FIG. 3: Norm convergence of the state-vector $(G, G^+, G^-, G^\theta, U, U^+, U^-, U^\theta)$ in axial symmetry with the norm (69), starting with 80 grid points in r, 16 in θ and 4 in ϕ and increasing the resolution by a factor of $p = 1.5$. Even though we are evolving axially symmetric data, four points in ϕ are needed for the boundary conditions, which have two ghost zones. We see that the convergence factor approaches 2, as anticipated for second-order finite differences approximation, which indicates a successful result.

8. DISCUSSION

8.1. Summary

This work represents a first step toward the implementation of the hyperboloidal approach to solving problems numerically in full GR. This approach will allow for more accurate results than the currently employed methods since it allows for the computation of the GW all the way out to $\mathscr{I}^+$, where they are unambiguously defined, via a smooth slice.

We took the linearized EFE in GHG and, by a careful choice of gauge source functions and constraint additions, showed that linearized GR can be modeled by the GU model, which allows us to understand the rate of decay of the fields and therefore how they should be rescaled such that they attain the expected limit at future null infinity. We also explored how our choice of gauge relates to the usual TT gauge.

By performing a hyperboloidal compactification and properly rescaling the fields, we derived regular equations at future null infinity. In fact, the rescaled fields are the relevant quantities to compute, since they are the radiation fields that we measure experi-

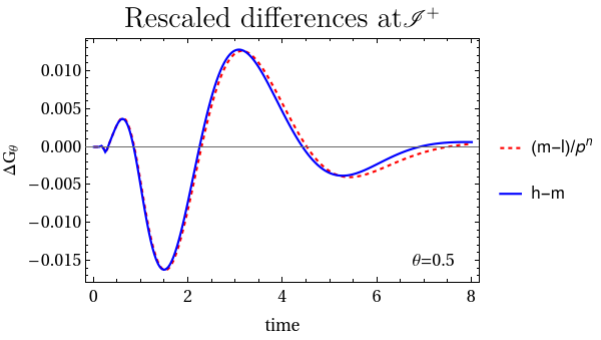

FIG. 4: Rescaled differences at $\mathscr{I}^+$ with $\theta = 0.5$ for the G_θ field. Starting with 80 grid points in the radial coordinate, 16 in θ and 4 in ϕ, the resolution was increased by a factor of $p = 1.5$. Even though we are evolving axially symmetric data, four points in ϕ are needed for the boundary conditions, which have two ghost zones. The evolution was performed with second-order finite differencing approximation of spatial derivatives, i.e. $n = 2$. l, m, and h stand for the values of the corresponding field given by the low, medium, and high-resolution runs, respectively. The alignment of the rescaled differences indicates convergence at $\mathscr{I}^+$.

mentally.

The regularity conditions at the origin were also derived, and we stress the importance of requiring that the evolved variables be sufficiently smooth functions of the coordinates.

Using NRPy+, the model equations were implemented in hyperboloidal coordinates on a staggered grid using axially symmetric initial data, in first-order in time and first-order in space. The results of our experiment were successful, as indicated by the norm and pointwise convergence tests.

8.2. Future work

Continuing work in the direction of treating future null infinity numerically, the next step is to evolve initial data in the absence of symmetries and show convegence. The generalization to full 3D implies that the fields g_ϕ and u_ϕ are no longer zero. Additional problems arise from this, since the ϕ component of terms with the divergence of g_A and u_A on the 2-sphere have an additional factor of $\frac{1}{\sin^2\theta}$, which diverges for $\theta = 0, \pi$.

Better results could be obtained by implementing the equations numerically using a non-staggered grid, thus avoiding extrapolation errors when computing the value of the fields at $\mathscr{I}^+$. Furthermore, better grids should be included in NRPy+ in the near future so the treatment of the origin might be simpler in the future.

Although we expect similar results for the linearized GR equations that we derived (since they can be indeed modeled by the GU equations), it would still be interesting to solve the linearized GR equations themselves, to verify and give more evidence of the correctness of our results. To do this, one would have to put together a careful match of the regularity conditions at the origin and at $\mathscr{I}^+$.

We could also expand this work by linearizing around different backgrounds (for instance, Schwarzschild and Kerr). Essentially, that implies changing the background quantities in Eq. (18) and following the same steps afterwards. In some aspects evolving around these backgrounds might be simpler, because, since we excise the BH interior, we do not have to deal with the origin.

Hyperboloidal evolution will be completely set up when all these results have been successfully generalized to full GR. Another field that needs to be included in the model is the *bad* field from the GBU model introduced in section 3. *Bad* fields are called "bad" because they decay slower than the others (their behavior grows with $\log(R)$).

There is good reason to believe that the hyperboloidal approach could be used in the future to obtain more accurate waveforms of GW for binary BH simulations, thus contributing to better measurements of the properties of the sources. Finally, being able to introduce matter in these simulations in order to evolve neutron stars or accretion disks, with the advantage of being able to reach future null infinity, would be the last effort to have a complete approach.

Bibliography

[1] D. Castelvecchi and A. Witze, Nature ("2016"), URL `https://doi.org/10.1038/nature.2016.19361`.

[2] B. P. Abbott et al. (LIGO Scientific, Virgo), Phys. Rev. Lett. **116**, 061102 (2016), 1602.03837.

[3] J. Sakstein and B. Jain, Phys. Rev. Lett. **119**, 251303 (2017), 1710.05893.

[4] A. Zenginoglu, J. Comput. Phys. **230**, 2286 (2011), 1008.3809.

[5] M. Duarte, J. Feng, E. Gasperin, and D. Hilditch, Class. Quant. Grav. **38**, 145015 (2021), 2101.07068.

[6] V. Mewes, Y. Zlochower, M. Campanelli, I. Ruchlin, Z. B. Etienne, and T. W. Baumgarte, Phys. Rev. D **97**, 084059 (2018), 1802.09625.

[7] D. Hilditch, E. Harms, M. Bugner, H. Rüter, and B. Brügmann, Class. Quant. Grav. **35**, 055003 (2018), 1609.08949.

[8] E. Gasperin, S. Gautam, D. Hilditch, and A. Vañó Viñuales, Class. Quant. Grav. **37**, 035006 (2020), 1909.11749.

[9] I. Ruchlin, Z. B. Etienne, and T. W. Baumgarte, Phys. Rev. D **97**, 064036 (2018), 1712.07658.

[10] H.-O. Kreiss and J. Oliger, *Methods for the approximate solution of time dependent problems*, 10 (International Council of Scientific Unions, World Meteorological Organization, 1973).

[11] C. R. Evans, Numerical Astrophysics p. 216 (1985).

[12] C. Gundlach, J. M. Martin-Garcia, and D. Garfinkle, Class. Quant. Grav. **30**, 145003 (2013), 1010.2427.

[13] I. Suárez Fernández, R. Vicente, and D. Hilditch, Phys. Rev. D **103**, 044016 (2021), 2007.13764.

[14] S. Gautam, A. Vañó Viñuales, D. Hilditch, and S. Bose, Phys. Rev. D **103**, 084045 (2021), 2101.05038.